NANO LETTERS

pubs.acs.org/NanoLett

Letter

Influence of Light Atoms on Quantification of Atomic Column Positions in Distorted Perovskites with HAADF-STEM

Michelle A. Smeaton, Noah Schnitzer, Hong Zheng, J. F. Mitchell, and Lena F. Kourkoutis*

Cite This: *Nano Lett.* 2023, 23, 6393−6398

Read Online

ACCESS | Metrics & More | Article Recommendations | Supporting Information

ABSTRACT: Measurement of picometer-scale atomic displacements by aberration-corrected STEM has become invaluable in the study of crystalline materials, where it can elucidate ordering mechanisms and local heterogeneities. HAADF-STEM imaging, often used for such measurements due to its atomic number contrast, is generally considered insensitive to light atoms such as oxygen. Light atoms, however, still affect the propagation of the electron beam in the sample and, therefore, the collected signal. Here, we demonstrate experimentally and through simulations that cation sites in distorted perovskites can appear to be displaced by several picometers from their true positions in shared cation−anion columns. The effect can be decreased through careful choice of sample thickness and beam voltage or can be entirely avoided if the experiment allows reorientation of the crystal along a more favorable zone axis. Therefore, it is crucial to consider the possible effects of light atoms and crystal symmetry and orientation when measuring atomic positions.

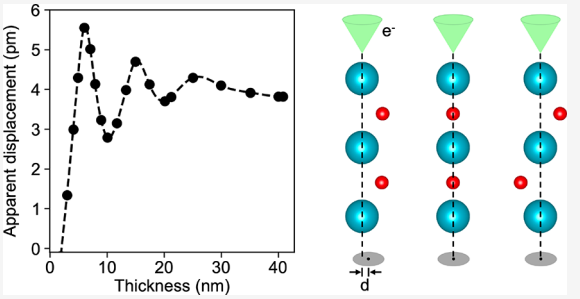

KEYWORDS: *lattice distortion, distorted perovskite, charge density wave, HAADF-STEM, electron channeling, oxygen octahedra*

With the introduction and proliferation of aberration correction, scanning transmission electron microscopy (STEM) has become an immensely powerful technique for studying the atomic structure of materials. Picometer-scale atomic displacements dictate the functional properties of many crystalline compounds, including quantum materials, ferroelectrics, and other multiferroics. The ability to resolve these subtle structural changes with STEM has provided real-space insight into ferroelectric order, periodic lattice distortions, and more.[1−5] In combination with other STEM modalities, high-resolution imaging can help elucidate the connections among charge, spin, lattice, and orbital degrees of freedom.

High-angle annular dark-field (HAADF)-STEM imaging is commonly used for atomic displacement measurements. Due to its strong atomic number (Z) dependence, HAADF-STEM imaging is often considered to be insensitive to light atoms such as oxygen. In atomic columns containing mixtures of heavy and light atoms, however, electron channeling—the behavior of the electron probe to be focused onto an atomic column in crystals oriented close to a high-symmetry zone axis—will be affected by both the light and the heavy atoms. The presence of light atoms in such atomic columns can, therefore, modify the collected signal. Channeling of the electron beam as it travels through a crystal has long been understood to have a strong effect on image contrast, and significant work has been undertaken to better understand the subtleties of its behavior.[6−11] In atomic columns that are not coherent or that have close neighboring columns, the channeling behavior can be particularly complex. A recent study combining multislice simulation and experimental HAADF-STEM showed that channeling can cause unintuitive contrast in noncoherently stacked heavy atomic columns based on crystal thickness and lateral separation of atomic sites.[12] Other studies have shown that light species, such as oxygen, in columns near heavy atomic columns can affect the radial intensity profile and even the shape of the heavy atomic column.[13−15] Here, we show experimentally that cation sites in a distorted perovskite oxide crystal can appear to be displaced by several picometers from their true positions in HAADF-STEM due to coherently displaced oxygen atoms in the same atomic columns. We then examine the channeling behavior that causes the apparent displacement using multislice simulations and consider ways to mitigate or avoid the artifact. Although we focus on a distorted perovskite oxide compound, we note that the electron channeling effects discussed here may contribute similar considerations across a wide range of light element-containing compounds, including, for example, sulfides and nitrides.

Experimental HAADF-STEM imaging was performed using accelerating voltages of 120 and 300 kV, with 21.4 and 30.3

Received: March 24, 2023
Revised: June 23, 2023
Published: July 10, 2023

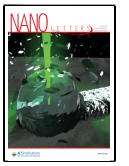

https://doi.org/10.1021/acs.nanolett.3c01140
Nano Lett. 2023, 23, 6393−6398

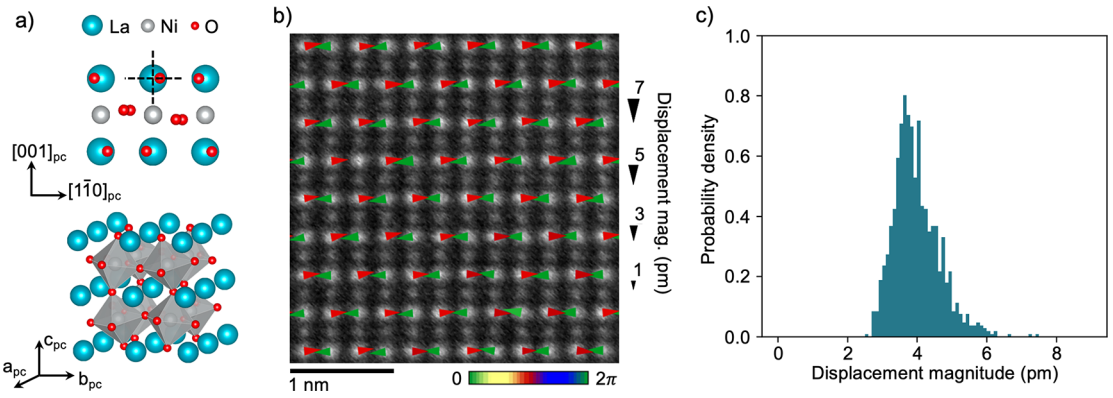

Figure 1. (a) Crystal structure of $LaNiO_3$ showing coherent oxygen atom displacements with respect to the lanthanum atoms in the $[110]_{pc}$ projection. (b) HAADF-STEM image acquired along the $[110]_{pc}$ projection using an accelerating voltage of 120 kV, with overlaid arrows representing the measured displacements of lanthanum−oxygen atomic columns with respect to the crystallographic positions of the lanthanum atoms. (c) Histogram of lanthanum−oxygen column displacements as shown in (b) for a 12 × 12 nm field of view. Panel (b) is presented with an alternate color scheme in Figure S3.

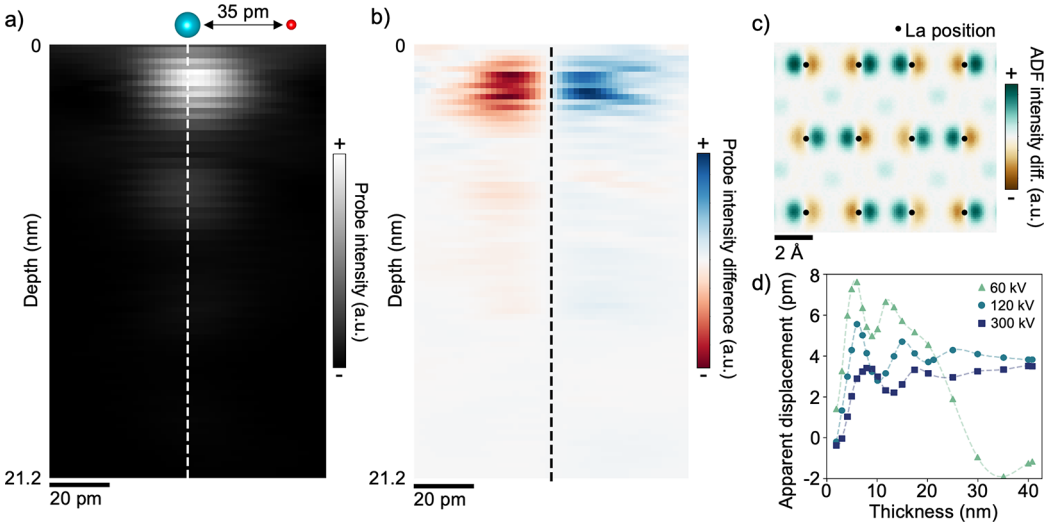

Figure 2. (a) Cross section of the simulated probe intensity as a function of crystal depth for a probe centered on a lanthanum column in $[110]_{pc}$-oriented $LaNiO_3$ with an accelerating voltage of 120 kV. The white dashed line represents the initial probe position, and the lanthanum and oxygen positions are shown at the top in teal and red, respectively. (b) Difference between the probe intensity cross section in (a) and the perpendicular cross section in which the lanthanum and oxygen atoms are aligned horizontally when projected onto the plane. The difference map shows a clear shift in probe intensity toward the oxygen atoms as the electron beam propagates through the crystal. (c) Difference between simulated HAADF-STEM images of $LaNiO_3$ with and without oxygen atoms included, showing that the oxygen atoms cause a shift in the HAADF signal away from the crystallographic lanthanum positions and toward the oxygen positions. (d) Lanthanum displacement as a function of crystal thickness measured from simulated HAADF-STEM images for accelerating voltages of 60, 120, and 300 kV, showing that a higher accelerating voltage reduces the apparent lanthanum displacements for nearly every thickness. Note the behavior above ~20 nm for 60 kV is more complicated, likely due to guaranteed multiple scattering.

mrad convergence angles, respectively. Imaging was performed on an aberration-corrected Thermo Fisher Scientific (TFS) Titan Themis and a TFS Spectra 300 X-CFEG. Electron transparent TEM lamellas of rhombohedral ($R\bar{3}m$) lanthanum nickelate ($LaNiO_3$) were prepared using a TFS Helios G4 X focused ion beam (FIB) from a bulk single crystal synthesized using a recently reported high oxygen pressure floating zone method.[16] See the Supporting Information for full experimental details.

Figure 1a shows a 3D model of $LaNiO_3$ and the same model projected down a [110] pseudocubic (pc) axis. In each lanthanum−oxygen column of the $[110]_{pc}$ projection, the oxygen sites are coherently displaced by 35 pm with respect to the lanthanum sites in the plane of the projection. The naive assumption that HAADF-STEM is insensitive to oxygen would suggest that the lanthanum columns would appear at their expected crystallographic positions, unaffected by the relatively displaced oxygen atoms. Experimentally, we find that this is not the case. An HAADF-STEM image of $LaNiO_3$ in the $[110]_{pc}$ orientation is shown in Figure 1b. The overlaid arrows, which indicate the measured displacement of each lanthanum column from its true lattice position, show that there is a distinct shift due to the presence of the coherently displaced oxygen atoms, as will be shown below. The displacements were extracted using an atom-tracking technique developed for the study of periodic lattice displacements (see Supporting Information).[17] A histogram of the displacement magnitudes is included in Figure 1c, showing an average apparent displacement of 3.7 pm.

https://doi.org/10.1021/acs.nanolett.3c01140
Nano Lett. 2023, 23, 6393−6398

To understand the origin and details of these apparent displacements, the propagation of the electron wave function through the $LaNiO_3$ crystal was simulated using the frozen-phonon multislice method.[18−20] All simulations were carried out using the TEMSIM simulation package[21] with 20 frozen phonon configurations. Figure 2a shows a cross section of the probe intensity as a function of depth through the crystal for a probe positioned on a lanthanum column. The positions of the lanthanum and oxygen columns are shown at the top of the panel. There is a visible shift in the probe intensity from the lanthanum position toward the oxygen position as the probe propagates within the first few nanometers of the crystal.

This shift is made clearer in Figure 2b, which shows the difference between the cross section in Figure 2a and the perpendicular cross section for which the lanthanum and oxygen atoms are aligned horizontally in the plane of the cross section. Since the HAADF-STEM intensity produced by an atom is proportional to the electron probe intensity at that atom position, this shift means that the collected intensity for a probe positioned on the lanthanum column will be reduced by the presence of the displaced oxygen atoms. Similarly, for a probe positioned 35 pm from a lanthanum column on the oxygen column, the presence of the oxygen atoms allows the probe intensity to channel onto the lanthanum column more effectively than for a probe positioned 35 pm from the lanthanum column, directly opposite the oxygen column (see Supporting Information), thus leading to greater HAADF intensity for that probe position. Taken together, these probe intensity simulations indicate that an HAADF-STEM image of $LaNiO_3$ oriented as shown in Figure 1a should show lanthanum positions shifted with respect to their true positions, consistent with the experimental measurements.

This result is further confirmed by full image simulations. Figure 2c shows the difference between a simulated HAADF-STEM image of $[110]_{pc}$-oriented $LaNiO_3$ and a simulated image of the same structure with all of the oxygen atoms removed. The positive (blue-green) intensity next to each lanthanum position matches the displacement direction of the oxygen atoms in the column. The measured displacement of the lanthanum−oxygen columns with respect to the true lanthanum positions is plotted as a function of the crystal thickness in Figure 2d. At 120 kV, the apparent displacement increases sharply in the first 5 nm of the crystal and then oscillates in accordance with the channeling signal, finally flattening out at a thickness of around 40 nm. Although the simulations are not designed to quantitatively match the experimental conditions, the experimentally measured displacement, 3.7 pm, is well within the range of displacements measured from simulation.

While the displacements measured from both simulation and experiment are significantly lower than the actual displacement of the oxygen sites, 35 pm, they are on the order of lattice displacements measured in quantum materials such as $LuFe_2O_{4+\delta}$ and $Bi_{1-x}Sr_{x-y}Ca_yMnO_3$ and ferroelectrics such as $Ba_{1-x}Sr_xTiO_3$.[22−24] It is therefore crucial to understand the possible effects of these channeling-induced apparent displacements when attempting to quantify the lattice modulations in such structures. Practically, this means identifying strategies to mitigate or avoid the effect during measurements.

In some distorted perovskite structures, the symmetry is such that no orientation will contain coherently displaced oxygen atoms in shared metal−oxygen columns, and in other structures, careful choice of the zone axis can allow one to avoid these channeling artifacts. For any $\langle 100\rangle_{pc}$-type zone axis, there will necessarily be no shared metal−oxygen columns with coherently displaced oxygen atoms, because these orientations are parallel to the axes of the octahedra. For $\langle 110\rangle_{pc}$-type zone axes, whether a particular crystal contains coherently displaced oxygen atoms is dictated by the tilt system of the oxygen octahedra as defined by Glazer notation.[25,26] Any structure with a tilt system comprising only zero or positive sense tilts, for example: $a^0a^0c^+$ or $a^+b^+b^+$, will have no zone axes with coherently displaced oxygen atoms. On the other hand, any structure with a tilt system containing one or more negative sense tilts will have zone axes with coherently displaced oxygen sites. In particular, any negative sense tilt axis will lead to coherently displaced oxygen sites along any zone axis not orthogonal to the negative sense tilt axis. For example, in a structure with an $a^0a^0c^-$ tilt system, the $[101]$, $[10\bar{1}]$, $[011]$, and $[01\bar{1}]$ pseudocubic zone axes will have coherently displaced oxygen atoms.

Examples of tilt systems with and without coherently displaced oxygen atoms in metal−oxygen columns are depicted in Figure 3 in perspective view as well as oriented down the $[001]_{pc}$ and $[101]_{pc}$ zone axes. In each structure, octahedra are colored according to their direction of rotation. In the model for tilt system $a^0a^0c^+$, shown in the left column, the rotations of successive octahedra along the $[001]_{pc}$ zone axis are matching, which leads to successive octahedra along the $[101]_{pc}$ zone axis being opposite, ensuring that there are no coherently displaced

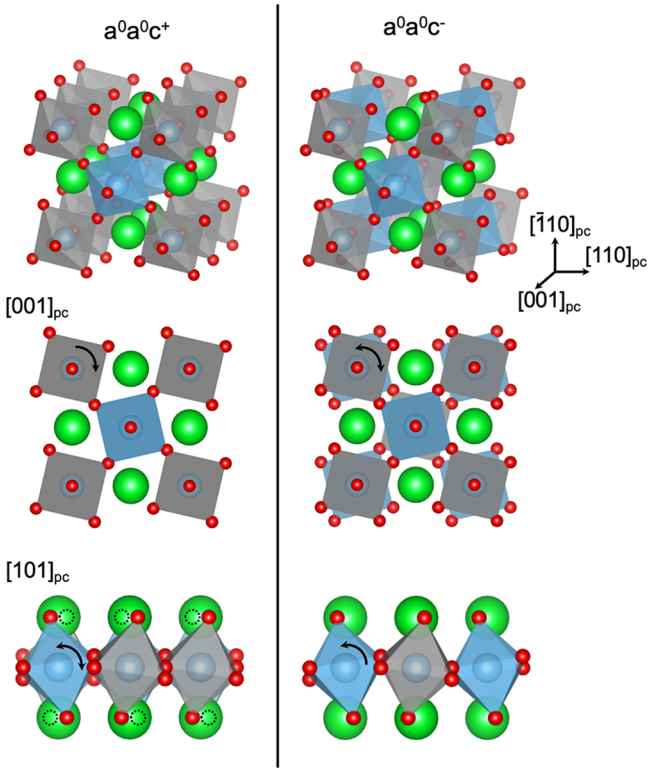

Figure 3. Examples of $a^0a^0c^+$ and $a^0a^0c^-$ tilt systems in a perspective view as well as projected down their $[001]_{pc}$ and $[101]_{pc}$ zone axes. Oxygen octahedra are colored according to their rotation direction (gray - clockwise, blue - counterclockwise). For the $a^0a^0c^+$ tilt system, the oxygen octahedra alternate their rotation direction along the $[101]_{pc}$ direction, while in the $a^0a^0c^-$ tilt system, the octahedral rotations are aligned in that direction, leading to coherently displaced oxygen atoms in lanthanum−oxygen columns.

https://doi.org/10.1021/acs.nanolett.3c01140
Nano Lett. 2023, 23, 6393−6398

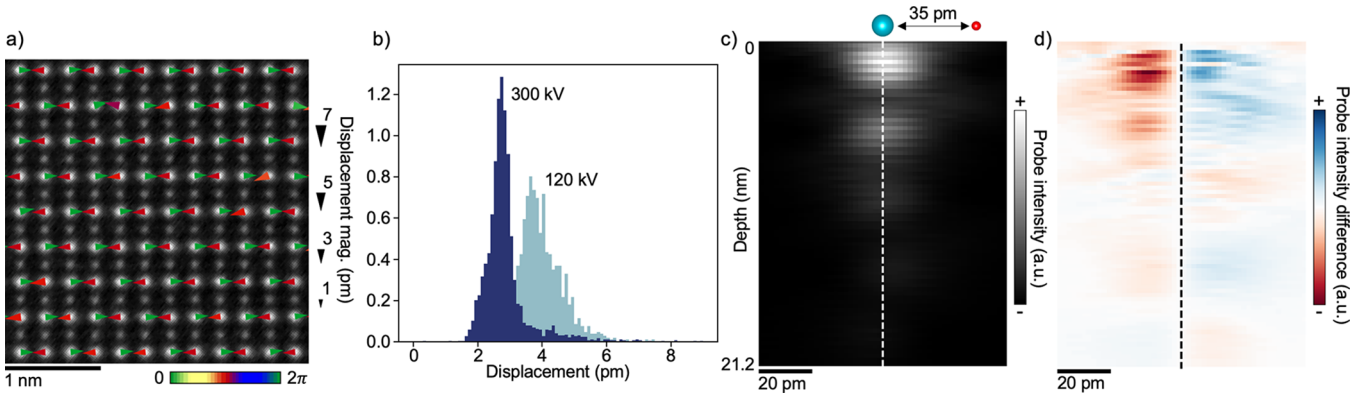

Figure 4. (a) Experimental HAADF-STEM image acquired along the $[110]_{pc}$ projection using a 300 kV accelerating voltage, with overlaid arrows representing the measured displacements of lanthanum−oxygen atomic columns with respect to the crystallographic positions of the lanthanum atoms. (b) Histogram of lanthanum−oxygen displacements as shown in a for a 20 nm × 20 nm field of view, with the histogram of displacements at 120 kV from Figure 1b included for comparison. (c,d) Cross section of the simulated probe intensity (c) and difference between the probe intensity cross section in c and the perpendicular cross section (d) for a probe positioned on a lanthanum column at 300 kV. Panel (a) is presented with an alternate color scheme in Figure S3.

oxygen atoms along that zone axis. The opposite is true for the $a^0a^0c^-$ tilt system, as shown in the right column. Here the octahedra match tilt direction in columns along the $[101]_{pc}$ zone axis, and thus, the oxygen atoms are displaced coherently along that axis.

In structures where a desired measurement requires data to be taken along a zone axis with coherently displaced oxygen atoms in metal−oxygen columns, the apparent displacement due to the oxygen atoms can be reduced by working at a higher accelerating voltage. This is observed experimentally, as shown in Figure 4a,b. Figure 4a shows an experimental image analogous to that shown in Figure 1b, but acquired at 300 kV, and overlaid with the measured displacements of the lanthanum−oxygen columns. A histogram of these displacements is presented in Figure 4b along with the histogram for 120 kV, showing that the average apparent displacement is decreased from 3.7 pm at 120 kV to 2.8 pm at 300 kV.

This dependence on voltage was also confirmed through simulations. Similar to Figure 2a,b, Figure 4c shows a cross section of the probe intensity through the lanthanum−oxygen column as a function of depth for a probe positioned on the lanthanum column, and Figure 4d shows the difference between that cross section and the perpendicular cross section in which the lanthanum and oxygen columns are aligned in the plane of the cross section. The shift in probe intensity visible in Figure 4c,d is notably less than that in Figure 2a,b. In particular, the first lobe in the probe intensity cross-section extends further to the right (toward the oxygen column) in Figure 2a than in Figure 4c. The voltage dependence is further confirmed by the simulated apparent displacement versus depth curves shown in Figure 2d for 60, 120, and 300 kV, wherein the displacement decreases with an increasing voltage consistently for nearly all thicknesses. At both 120 and 300 kV, the channeling oscillations flatten out by ∼40 nm. At 60 kV, the channeling behavior is more complex for thicknesses greater than ∼25 nm, likely due to the guaranteed multiple scattering at those thicknesses. See Supporting Information for further discussion.

Even at 300 kV, the apparent displacements due to coherently displaced oxygen atoms are non-negligible. Therefore, care should be taken when interpreting atomic-position measurements of such data. In some cases, the effects of coherently displaced oxygen atoms can be separated from the lattice modulations of interest. Symmetry analysis can be used to determine whether the oxygen and cation displacement periodicities give rise to distinct Fourier peaks. If this is the case, the relevant peaks can be used to extract the atomic displacements associated with the modulation of interest, to the exclusion of the oxygen-channeling effects. This process is analogous to the separation of atomic displacements associated with two transverse periodic lattice displacements in charge ordered manganites.[17] Simulations could also be used in combination with thickness measurements and precise atom tracking to help disentangle the effects of cation and anion displacements. Previously, incorrect displacements of cation sites have also been observed resulting from specimen mistilt in combination with differing channeling strength in neighboring columns of different atomic species.[27] Specimen mistilt would also likely affect the magnitude of the apparent displacements due to coherently displaced oxygen atoms.

In summary, we have shown through experiment and simulation that HAADF-STEM images of distorted perovskites can exhibit anomalous atomic positions for mixed cation−anion columns containing coherently displaced anions due to electron channeling effects from the much lighter anions. We have demonstrated that the magnitude of the apparent displacement from the crystallographic position depends on the probe accelerating voltage and the crystal thickness. It is likely also affected by additional imaging parameters such as the convergence angle and specimen mistilt. These apparent displacements can skew measurements of atomic positions in a wide variety of functional oxides and other light element-containing compounds, such as sulfides and nitrides, across the fields of energy materials, multiferroics, quantum materials, and more. Indeed, the displacements demonstrated here are comparable to the magnitudes of lattice modulations associated with ferroelectricity and quantum phenomena, such as charge density waves. Given the recent increased interest in precise atomic-position measurements enabled by aberration-corrected STEM, it is crucial to remain cognizant of this effect and to consider avenues to avoid or reduce its impact.

https://doi.org/10.1021/acs.nanolett.3c01140
Nano Lett. 2023, 23, 6393−6398

■ ASSOCIATED CONTENT

Data Availability Statement

The data that support the findings of this study are available from the corresponding author upon reasonable request. Raw data related to the experimental STEM measurements have been deposited in the Platform for the Accelerated Realization, Analysis, and Discovery of Interface Materials (PARADIM) database and are available at https://data.paradim.org/.

Supporting Information

The Supporting Information is available free of charge at https://pubs.acs.org/doi/10.1021/acs.nanolett.3c01140.

Experimental details, additional discussion of channeling behavior at the oxygen position and at an accelerating voltage of 60 kV, experimental atomic displacement maps in an alternate color scheme. (PDF)

■ AUTHOR INFORMATION

Corresponding Author

Lena F. Kourkoutis − *School of Applied and Engineering Physics and Kavli Institute for Nanoscale Science, Cornell University, Ithaca, New York 14853, United States;* orcid.org/0000-0002-1303-1362; Email: lena.f.kourkoutis@cornell.edu

Authors

Michelle A. Smeaton − *Department of Materials Science and Engineering, Cornell University, Ithaca, New York 14853, United States;* orcid.org/0000-0001-9114-1009

Noah Schnitzer − *Department of Materials Science and Engineering, Cornell University, Ithaca, New York 14853, United States*

Hong Zheng − *Materials Science Division, Argonne National Laboratory, Lemont, Illinois 60439, United States*

J. F. Mitchell − *Materials Science Division, Argonne National Laboratory, Lemont, Illinois 60439, United States;* orcid.org/0000-0002-8416-6424

Complete contact information is available at: https://pubs.acs.org/10.1021/acs.nanolett.3c01140

Notes

The authors declare no competing financial interest.

■ ACKNOWLEDGMENTS

This work was primarily supported by the National Science Foundation [Platform for the Accelerated Realization, Analysis, and Discovery of Interface Materials (PARADIM)] under Cooperative Agreement No. DMR-2039380. It made use of the Cornell Center for Materials Research Shared Facilities, which are supported through the NSF MRSEC program (DMR-1719875). Additional support was provided by the Packard Foundation. Crystal growth was performed in the Materials Science Division of Argonne National Laboratory and sponsored by the U.S. DOE, Office of Science, Office of Basic Energy Sciences, Materials Science and Engineering Division. MAS and NS acknowledge additional support from the NSF GRFP under award number DGE-2139899. The authors thank Berit H. Goodge for helpful discussions.

■ REFERENCES

(1) Van Tendeloo, G.; Bals, S.; Van Aert, S.; Verbeeck, J.; Van Dyck, D. Advanced electron microscopy for advanced materials. *Adv. Mater.* **2012**, *24*, 5655−5675.

(2) MacLaren, I.; Ramasse, Q. M. Aberration-corrected scanning transmission electron microscopy for atomic-resolution studies of functional oxides. *International Materials Reviews* **2014**, *59*, 115−131.

(3) Minor, A. M.; Denes, P.; Muller, D. A. Cryogenic electron microscopy for quantum science. *MRS Bull.* **2019**, *44*, 961−966.

(4) Guo, H.; Saghayezhian, M.; Wang, Z.; Zhu, Y.; Zhang, J.; Plummer, W. Visualizing quantum phenomena at complex oxide interfaces: An atomic view from scanning transmission electron microscopy. *Frontiers of Physics* **2020**, *15*, 13401.

(5) Moore, K.; Bangert, U.; Conroy, M. Aberration corrected STEM techniques to investigate polarization in ferroelectric domain walls and vortices. *APL Materials* **2021**, *9*, 020703.

(6) Voyles, P. M.; Grazul, J. L.; Muller, D. A. Imaging individual atoms inside crystals with ADF-STEM. *Ultramicroscopy* **2003**, *96*, 251−273.

(7) Kourkoutis, L. F.; Parker, M. K.; Vaithyanathan, V.; Schlom, D. G.; Muller, D. A. Direct measurement of electron channeling in a crystal using scanning transmission electron microscopy. *Physical Review B - Condensed Matter and Materials Physics* **2011**, *84*, 1−7.

(8) Hovden, R.; Xin, H. L.; Muller, D. A. Channeling of a subangstrom electron beam in a crystal mapped to two-dimensional molecular orbitals. *Physical Review B - Condensed Matter and Materials Physics* **2012**, *86*, 1−7.

(9) Wu, R. J.; Mittal, A.; Odlyzko, M. L.; Mkhoyan, K. A. Simplifying electron beam channeling in scanning transmission electron microscopy (STEM). *Microscopy and Microanalysis* **2017**, *23*, 794−808.

(10) Lebeau, J. M.; Findlay, S. D.; Wang, X.; Jacobson, A. J.; Allen, L. J.; Stemmer, S. High-angle scattering of fast electrons from crystals containing heavy elements: Simulation and experiment. *Physical Review B - Condensed Matter and Materials Physics* **2009**, *79*, 2−7.

(11) Loane, R. F.; Kirkland, E. J.; Silcox, J. Visibility of single heavy atoms on thin crystalline silicon in simulated annular dark-field STEM images. *Acta Crystallogr., Sect. A* **1988**, *44*, 912−927.

(12) Yun, H.; Prakash, A.; Jalan, B.; Jeong, J. S.; Mkhoyan, K. A. STEM beam channeling in $BaSnO_3/LaAlO_3$ perovskite bilayers and visualization of 2D misfit dislocation network. *Ultramicroscopy* **2020**, *208*, 112863.

(13) Borisevich, A.; Ovchinnikov, O. S.; Chang, H. J.; Oxley, M. P.; Yu, P.; Seidel, J.; Eliseev, E. A.; Morozovska, A. N.; Ramesh, R.; Pennycook, S. J.; Kalinin, S. V. Mapping Octahedral Tilts and Polarization Across a Domain Wall in BiFeO3 from Z-Contrast Scanning Transmission Electron Microscopy Image Atomic Column Shape Analysis. *ACS Nano* **2010**, *4*, 6071−6079.

(14) Mostaed, A.; Balakrishnan, G.; Lees, M. R.; Yasui, Y.; Chang, L. J.; Beanland, R. Atomic structure study of the pyrochlore $Yb_2Ti_2O_7$ and its relationship with low-temperature magnetic order. *Physical Review B - Condensed Matter and Materials Physics* **2017**, *95*, 094431.

(15) Mostaed, A.; Walkley, B.; Hatnean, M. C.; Balakrishnan, G.; Lees, M. R.; Beanland, R.; Sinclair, D. C.; Reaney, I. M. Characterizing oxygen atoms in perovskite and pyrochlore oxides using ADF-STEM at a resolution of a few tens of picometers. *Acta Mater.* **2021**, *208*, 116717.

(16) Zhang, J.; Zheng, H.; Ren, Y.; Mitchell, J. F. High-pressure floating-zone growth of perovskite nickelate $LaNiO_3$ single crystals. *Cryst. Growth Des.* **2017**, *17*, 2730−2735.

(17) Savitzky, B. H.; El Baggari, I.; Admasu, A. S.; Kim, J.; Cheong, S. W.; Hovden, R.; Kourkoutis, L. F. Bending and breaking of stripes in a charge ordered Manganite. *Nat. Commun.* **2017**, *8*, 1−6.

(18) Cowley, J. M.; Moodie, A. F. The scattering of electrons by atoms and crystals. I. A new theoretical approach. *Acta Crystallogr.* **1957**, *10*, 609−619.

(19) Goodman, P.; Moodie, A. F. Numerical evaluations of *N*-beam wave functions in electron scattering by the multi-slice method. *Acta Crystallogr., Sect. A* **1974**, *30*, 280−290.

(20) Kirkland, E. J.; Loane, R. F.; Silcox, J. Simulation of annular dark field STEM images using a modified multislice method. *Ultramicroscopy* **1987**, *23*, 77−96.

(21) Kirkland, E. J. *Advanced computing in electron microscopy*, 3rd ed.; Springer Nature: Switzerland, 2020.
(22) Deng, S.; Wu, L.; Cheng, H.; Zheng, J. C.; Cheng, S.; Li, J.; Wang, W.; Shen, J.; Tao, J.; Zhu, J.; Zhu, Y. Charge-lattice coupling in hole-doped $LuFe_2O_{4+\delta}$: the origin of second-order modulation. *Phys. Rev. Lett.* **2019**, *122*, 126401.
(23) El Baggari, I.; Savitzky, B. H.; Admasu, A. S.; Kim, J.; Cheong, S.-W.; Hovden, R.; Kourkoutis, L. F. Nature and evolution of incommensurate charge order in manganites visualized with cryogenic scanning transmission electron microscopy. *Proc. Natl. Acad. Sci. U.S.A.* **2018**, *115*, 1445−1450.
(24) Damodaran, A. R.; et al. Large polarization gradients and temperature-stable responses in compositionally-graded ferroelectrics. *Nat. Commun.* **2017**, *8*, 14961.
(25) Glazer, A. M. The classification of tilted octahedra in perovskites. *Acta Crystallographica Section B* **1972**, *28*, 3384−3392.
(26) Glazer, A. M. Simple ways of determining perovskite structures. *Acta Crystallogr., Sect. A* **1975**, *31*, 756−762.
(27) Cui, J.; Yao, Y.; Wang, Y. G.; Shen, X.; Yu, R. C. The origin of atomic displacements in HAADF images of the tilted specimen. *Ultramicroscopy* **2017**, *182*, 156−162.

https://doi.org/10.1021/acs.nanolett.3c01140
Nano Lett. 2023, 23, 6393−6398